Supporting Information

Asymmetric Microdome Structure for Flexible and Skin-mountable Pressure Sensor with Computational Analysis

Yeoul Kang [‡a], Mary Kim [‡b], Seung Geun Jo [a], Jongmoon Jang [c], Sang-Jin Lee [d], Ki Jun Yu[*e], Sangryun Lee [*b] and Jung Woo Lee[*a]

a. Department of Materials Science and Engineering, Pusan National University, Busan, 46241, Republic of Korea. E-mail: jungwoolee@pusan.ac.kr

b. Department of Mechanical and Biomedical Engineering, Ewha Womans University, Seoul 03760, Republic of Korea. E-mail: sr.lee@ewha.ac.kr

c. Department of Electronic Engineering, Yeungnam University, Gyeongsan, 38541, Republic of Korea

d. School of Electronics Engineering, Chungbuk National University, Cheongju, 28644, Republic of Korea

e. School of Electrical and Electronic Engineering, Yonsei University, 50 Yonsei-ro, Seodaemungu, Seoul 03722, Republic of Korea. E-mail: kijunyu@yonsei.ac.kr

‡ These authors contributed equally to this work.

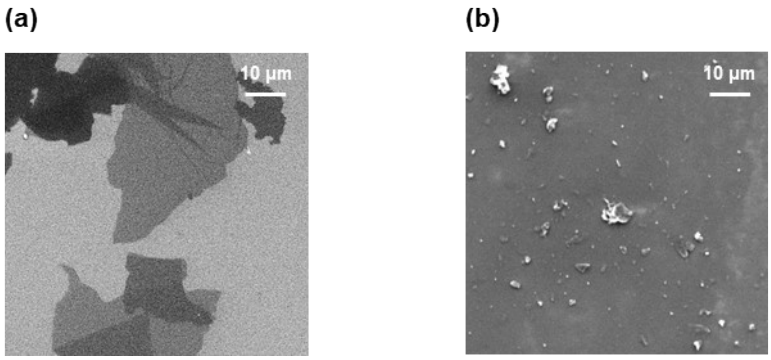

Fig. S1. SEM images of (a) LGO sheets and (b) SGO sheets.

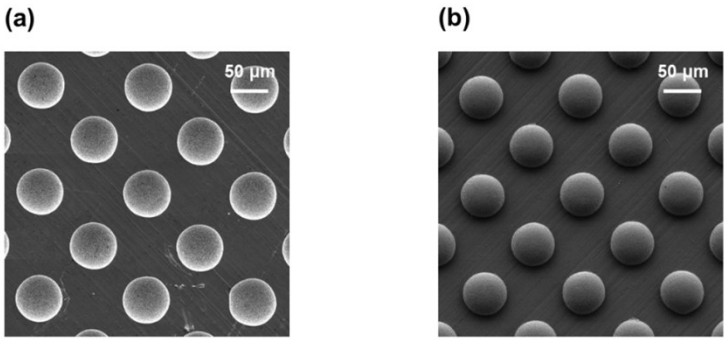

Fig. S2. SEM images of (a) patterned copper mold and (b) demolded md-PDMS.

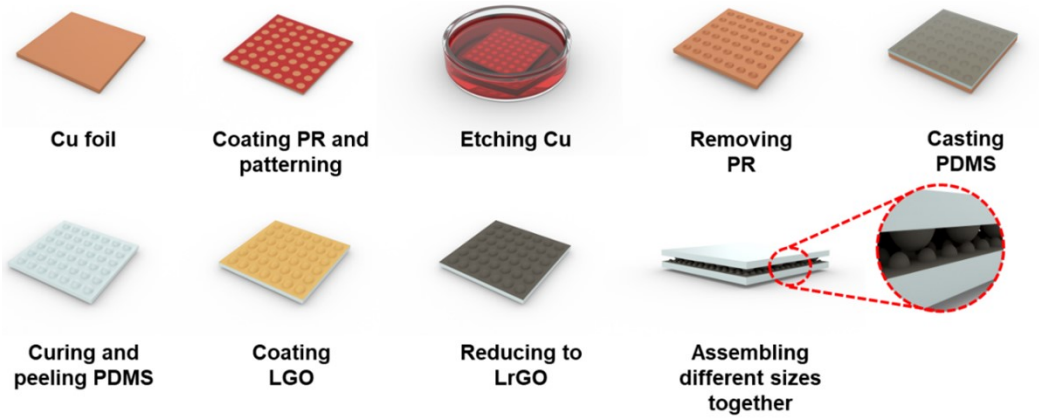

Fig. S3. Schematic illustration of fabrication process for AMS pressure sensor.

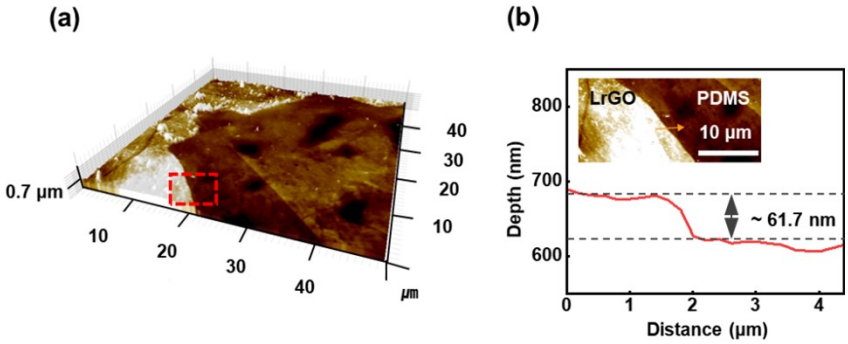

Fig. S4. (a) AFM 3D image of interface between LrGO coating layer and PDMS substrate. (b) Depth profile of the LrGO coating layer (inset: corresponding AFM 2D image).

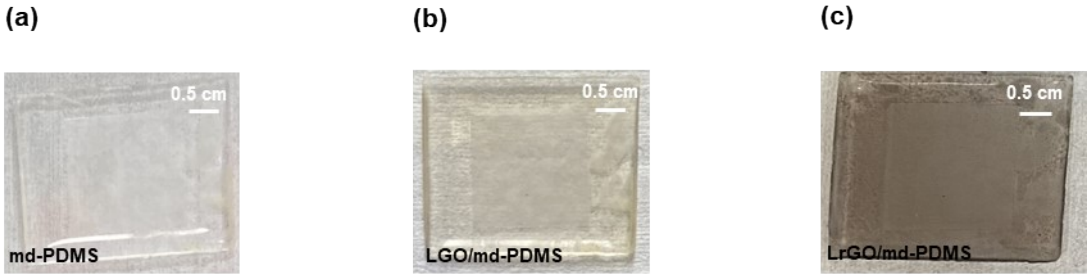

Fig. S5. Optical images of (a) md-PDMS, (b) LGO/md-PDMS, and (c) LrGO/md-PDMS.

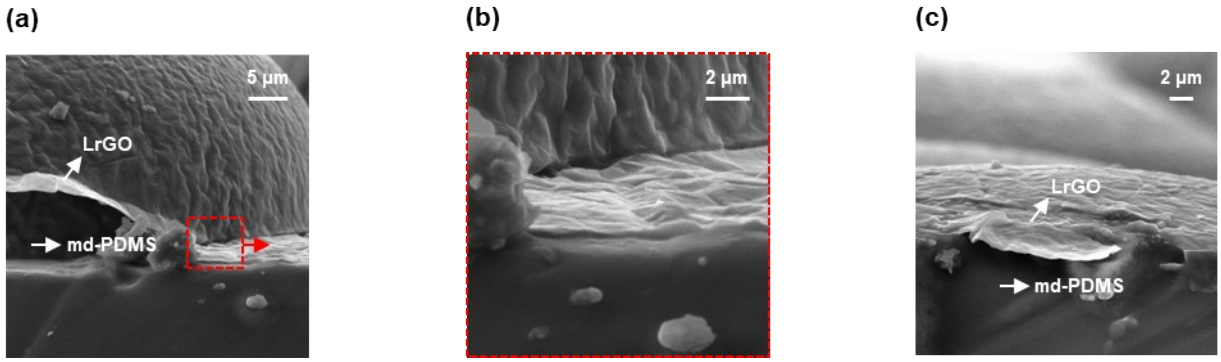

Fig. S6. Cross-sectional SEM images of (a) partially peeled LrGO coating layer on md-PDMS, (b) corresponding magnified view of LrGO/md-PDMS, and (c) LrGO coating layer on a vertically cut microdome within the md-PDMS.

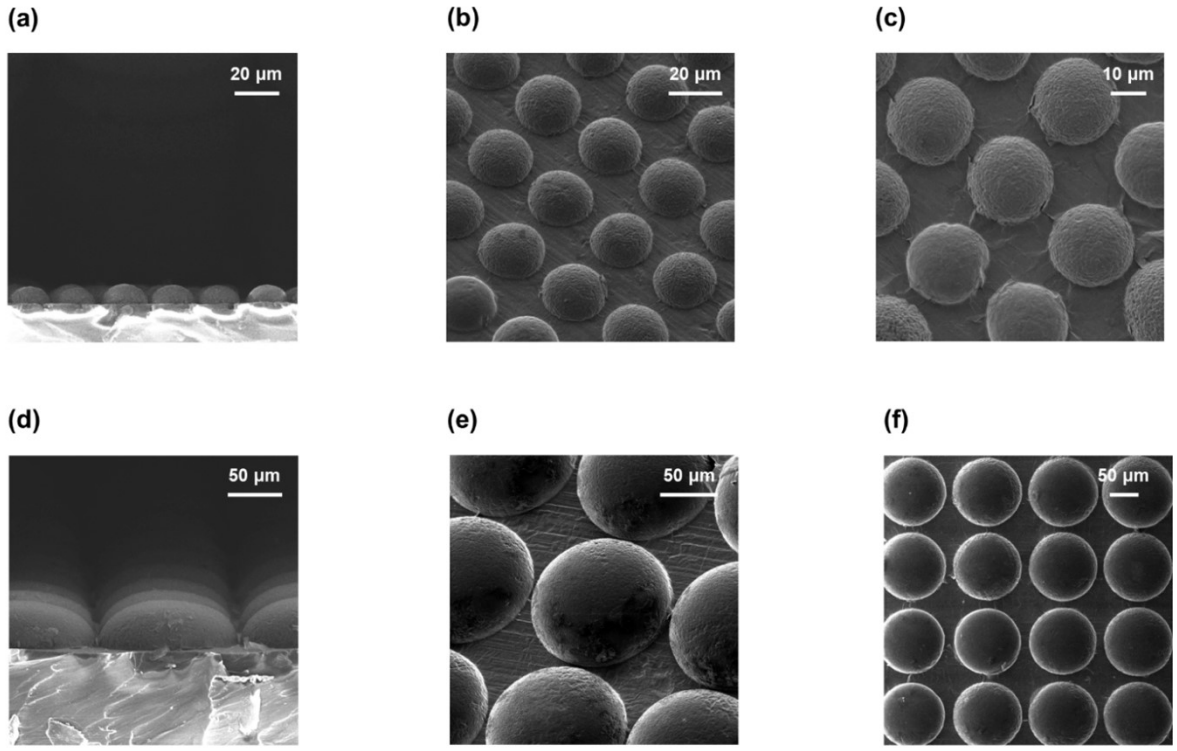

Fig. S7. SEM images of LrGO/md-PDMS for bottom layer: (a) Cross-sectional view, (b) Tilted view, (c) Planar view. SEM images of LrGO/md-PDMS for top layer: (a) Cross-sectional view, (b) Tilted view, (c) Planar view.

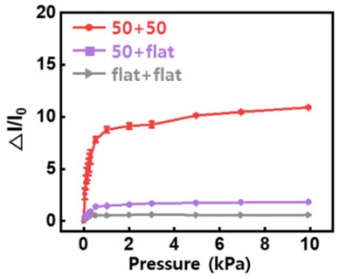

Fig. S8. Relative current variation of the pressure sensors with planar, single, interlocked microdome structure under the pressure range of 0−10 kPa**.**

(a)

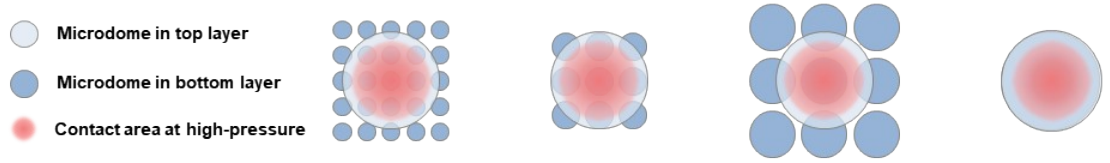

Radius of microdome (top+down) [μm]	50+10	50+15	50+25	50+50
Asymmetric ratio	5	3.3	2	1
Maximum number of contact microdomes	9	5	5	1

(b)

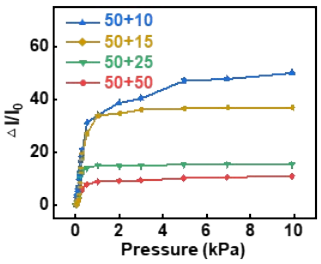

Fig. S9. (a) Schematic illustration of the number of contact microstructures for different asymmetric ratio. (b) Relative current variation of the pressure sensors with different asymmetric ratio under the pressure range of 0-10 kPa.

(a) (b)

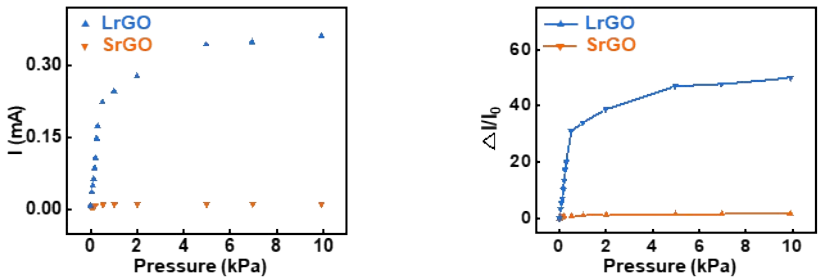

Fig. S10. (a) Current response and (b) relative current variation under increasing pressure for AMS pressure sensors with different sensing materials SrGO and LrGO.

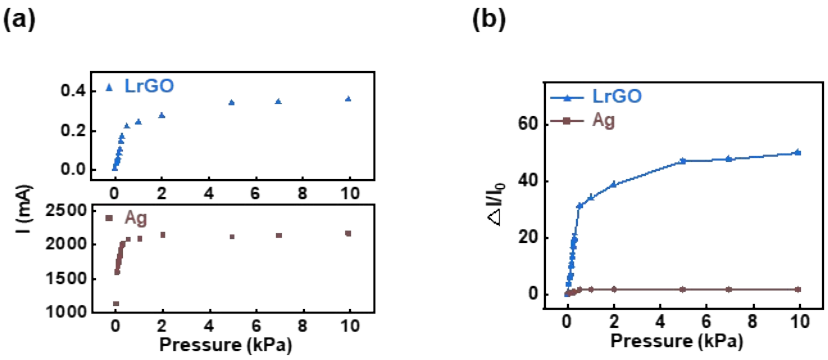

Fig. S11. (a) Current response and (b) relative current variation under increasing pressure for AMS pressure sensors with different sensing materials Ag and LrGO.

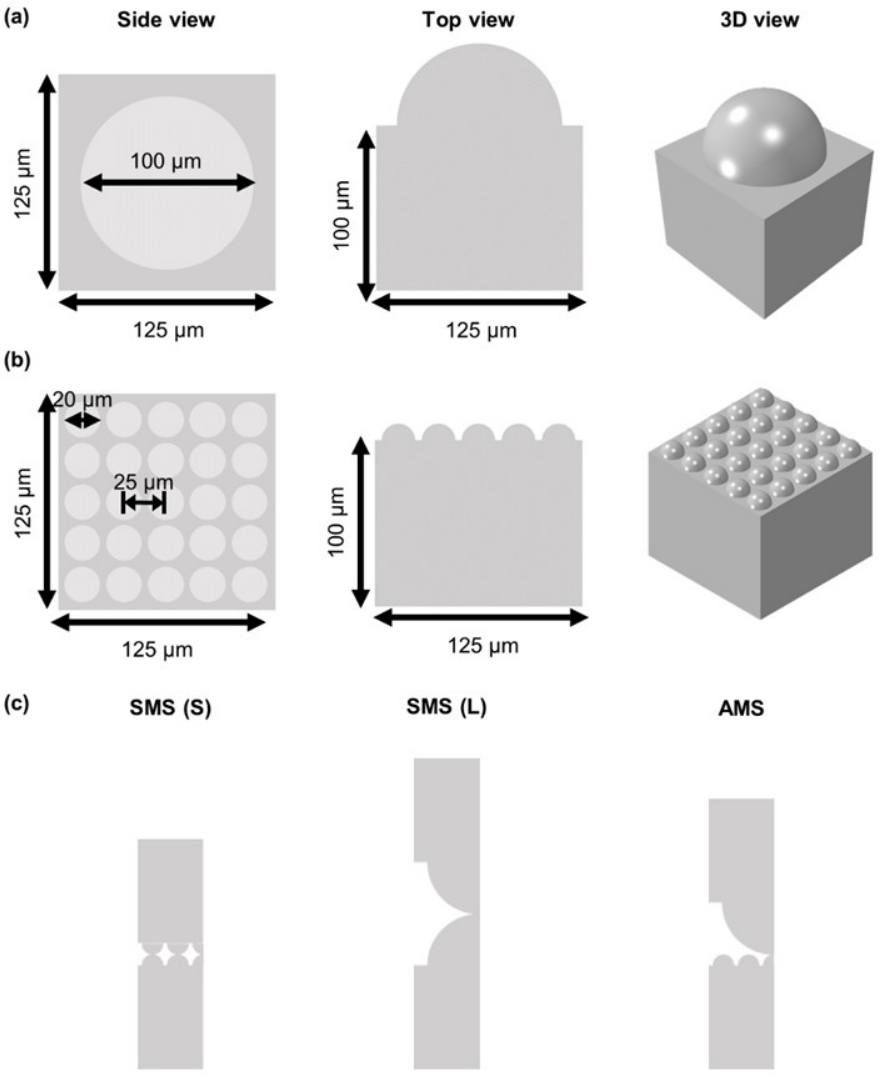

Fig. S12. FEM model: side view, top view, and 3D shape of a microdome with the radius of (a) 50 μm and (b) 10 μm placed on a substrate. (c) 2D view of SMS (S) and (L), and AMS.

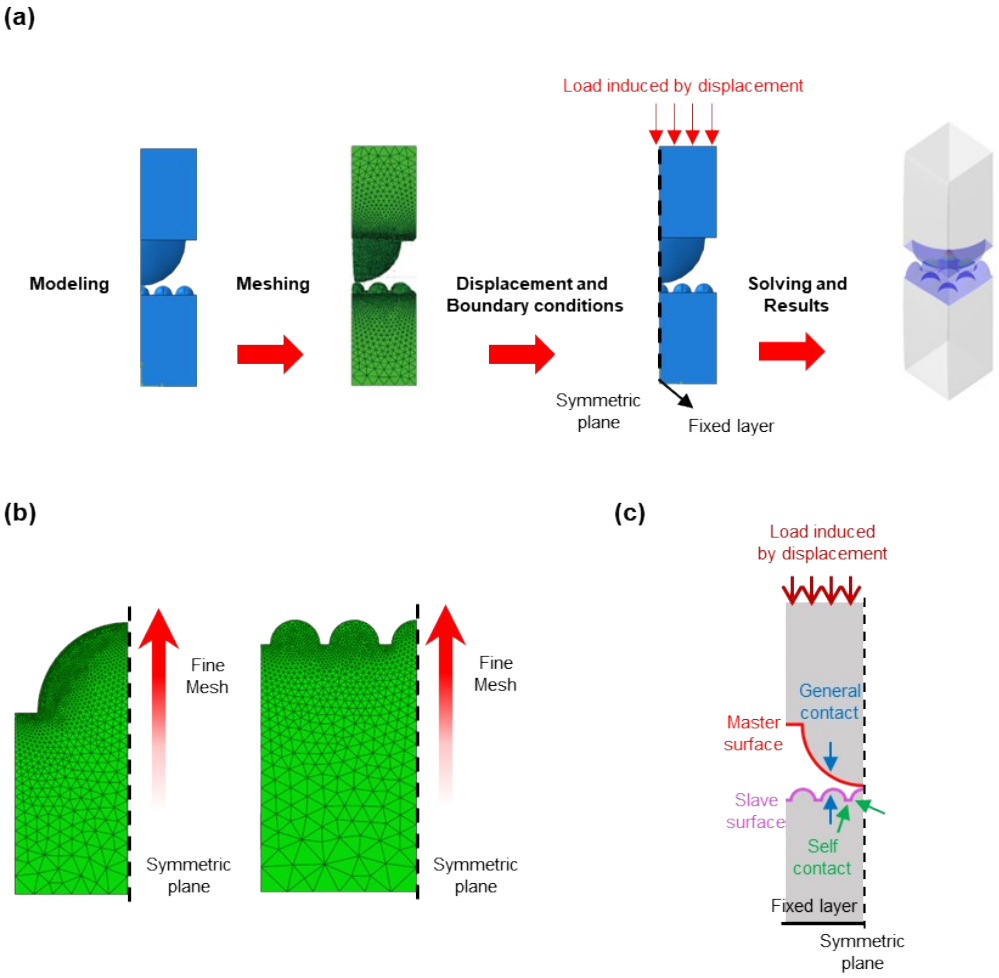

Fig. S13. (a) Main steps of finite element analysis. (b) Mesh shape of 1/4 microstructure with radius of 50 μm, (left) and 10 μm (right). (c) Displacement and boundary conditions in AMS.

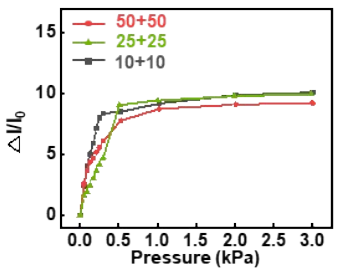

Fig. S14. Relative current variation under increasing pressure for SMS pressure sensors with different radius sizes.

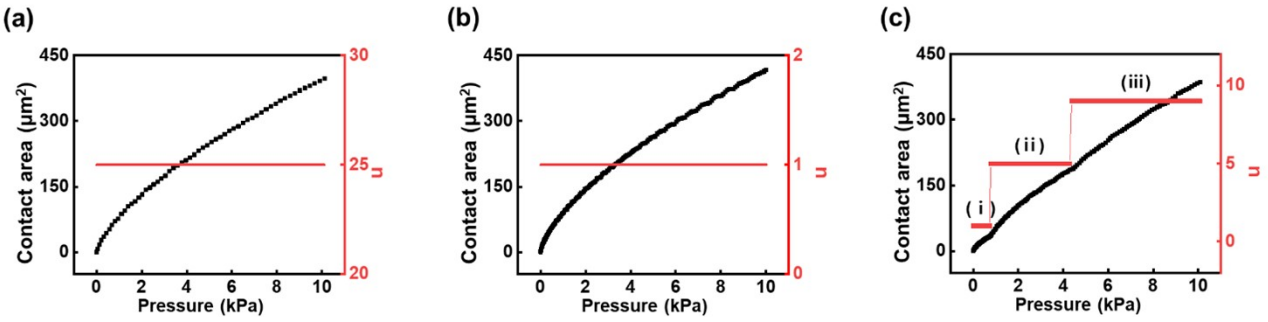

Fig. S15. Contact area and number of microstructures in contact responding to applied pressure for (a) SMS (S), (b) SMS (L) and (c) AMS calculated in FEM results .

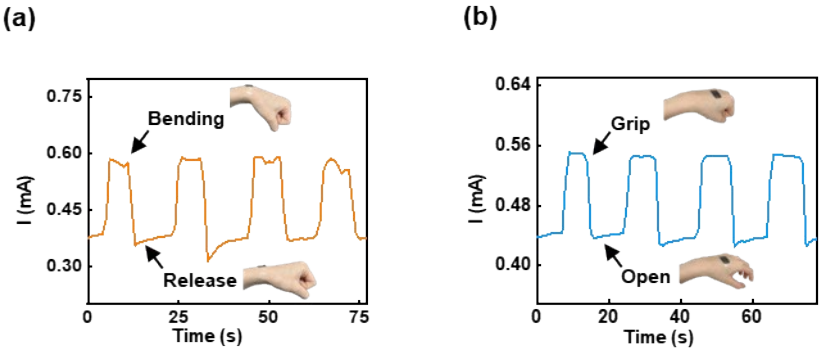

Fig. S16. Response of the sensor to various physiological activities of (a) wrist bending (inset) an optical image of the sensor attached onto the wrist joint, (b) hand gripping (inset) an optical image of the sensor attached onto the back of the hand.

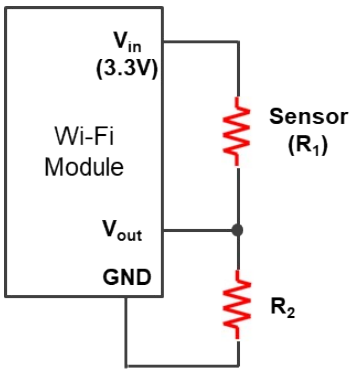

Fig. S17. Voltage divider circuit with Wi-Fi module for wireless monitoring.

Table 1. Comparison of piezoresistive sensor with different structures and fabrication method.

Sensitivity [kPa^{-1}]	**Pressure [kPa]**	**Structure**	**Method**	**Materials**	**Ref.**
1.2	< 25	Hierarchical structure	Lotus leaf molding	Graphene	[1]
4.48 0.86	< 22 27−65	Hierarchical microstructure	Laser	Ag NW	[2]
8.3 4.3 1.5	< 10 10−30 > 30	Ordered multilevel microstructure	Laser	CB-PU	[3]
35.51 11.71 3.54	< 0.25 0.25−4 < 23	Hierarchical structure	Laser	MWCNT	[4]
0.29 0.03 0.0033	< 1.6 1.6−7.8 7.8−70	Hierarchical Microspines structure	Abrasive paper molding	rGO/Mxene	[5]
50.45 4.35	< 0.05 0.05−0.4	Irregular microdome structure	Thermally expandable microspheres	Ti/Au	[6]
63.07 **1.96**	**< 0.5** **0.5−10**	Asymmetric microdome structure	Patterned copper mold	LrGO	**This work**

References

[1] J. Shi, L. Wang, Z. Dai, L. Zhao, M. Du, H. Li, Y. Fang, *Small* **2018**, 14, 1800819.

[2] Q. Du, L. Liu, R. Tang, J. Ai, Z. Wang, Q. Fu, C. Li, Y. Chen, X. Feng, *Advanced Materials Technologies* **2021**, 6, 2100122.

[3] D. Geng, S. Chen, R. Chen, Y. You, C. Xiao, C. Bai, T. Luo, W. Zhou, *Advanced Materials Technologies* **2022**, 7, 2101031.

[4] J. Li, T. Wu, H. Jiang, Y. Chen, Q. Yang, *Advanced Intelligent Systems* **2021**, 3, 2100070.

[5] J. Xu, L. Zhang, X. Lai, X. Zeng, H. Li, *ACS Applied Materials & Interfaces* **2022**, 14, 27262.

[6] Y. Jung, J. Choi, W. Lee, J. S. Ko, I. Park, H. Cho, *Advanced Functional Materials* **2022**, 32, 2201147.